Two-Step Reshaping of Acicular Gold Nanoparticles

Jieli Lyu, Lauren Matthews, Thomas Zinn, Damien Alloyeau, Cyrille Hamon, Doru Constantin

Two-step reshaping of acicular gold nanoparticles

Jieli Lyu,[ab] Lauren Matthews,[cd] Thomas Zinn,[ce]
Damien Alloyeau,[†f] Cyrille Hamon,[‡b] Doru Constantin,[*g]

Abstract

Anisometric plasmonic nanoparticles find applications in various fields, from photocatalysis to biosensing. However, exposure to heat or to specific chemical environments can induce their reshaping, leading to loss of function. Understanding this process is therefore relevant both for the fundamental understanding of such nano-objects and for their practical applications. We followed in real time the spontaneous reshaping of gold nanotetrapods in solution via optical absorbance spectroscopy, revealing a two-step kinetics (fast tip flattening into {110} facets, followed by slow arm shortening) with characteristic times a factor of six apart but sharing an activation energy around 1 eV. Synchrotron-based X-ray scattering confirms this time evolution, which is much faster in solution than in the dry state, highlighting the importance of the aqueous medium and supporting a dissolution-redeposition mechanism or facilitated surface diffusion. High-temperature transmission electron microscopy of the dry particles validates the solution kinetics.

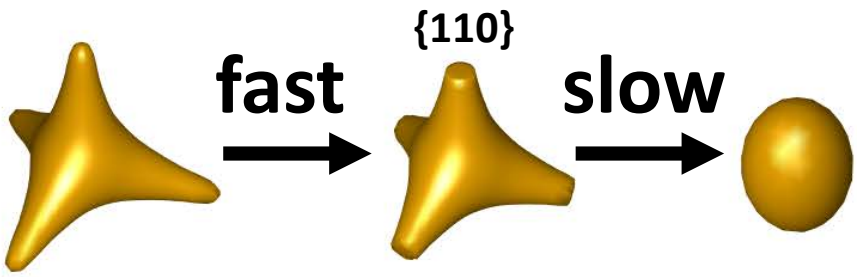

[a] *School of Materials Science and Engineering, Xi'an University of Technology, Xi'an 710048, Shaanxi, People's Republic of China*
[b] *Université Paris-Saclay, CNRS, Laboratoire de Physique des Solides, 91405 Orsay, France*
[c] *The European Synchrotron Radiation Facility, 38043 Grenoble CEDEX 9, France*
[d] *Present address: ISIS Neutron and Muon Source, Rutherford Appleton Laboratory, Chilton, OX11 0QX, United Kingdom*
[e] *Present address: Diamond Light Source, Didcot OX11 0DE, United Kingdom*
[f] *Laboratoire Matériaux et Phénomènes Quantiques, Université Paris Cité - CNRS, Paris, France*
[g] *Institut Charles Sadron, CNRS and Université de Strasbourg, 67034 Strasbourg, France*
[†] damien.alloyeau@u-paris.fr
[‡] cyrille.hamon@universite-paris-saclay.fr
[*] constantin@unistra.fr

1 Introduction

Acicular nanoparticles (NPs) (composed of a spherical core from which sharp-tipped arms radiate outwards) are thermodynamically unstable, so they are obtained in fast processes and often evolve into blunter objects[1]. Reliably synthesizing these NPs and stabilizing them against reshaping is important in view of applications, but can also yield insight into the evolution of metal surfaces, their interaction with ligands and so on. Among acicular NPs, nanotetrapods (NTPs)[2,3] are particularly interesting due to their well-defined tetrahedral structure, which results in strong second harmonic generation properties[4]. NTPs spontaneously reshape even at room temperature, making them a promising model for the study of morphological evolution. They are closely related to Au nanostars (NS)[5], whose reshaping has been studied in detail[6–8]. However, NS have a random distribution of short tips, making them less amenable to an overall morphological description and to quantitative analysis.

Studying the time evolution of NP morphologies is challenging: UV-Vis-IR absorbance spectroscopy (AS) is non-invasive, directly applicable in the reaction medium, has a very good time resolution and is thus universally used, in particular for noble metal objects whose plasmon resonances endow them with very specific absorbance bands. However, the absorbance spectra are only sensitive to some features and cannot yield the complete particle morphology. Synchrotron-based small-angle X-ray scattering (SAXS) shares the advantages of AS, while being more sensitive to the overall shape of the object. On the downside, it is much less available and data analysis is fairly involved, often requiring full-curve fitting in order to extract meaningful information. Imaging techniques such as liquid-phase transmision electron microscopy do exist, but only a few particles can be observed at a time and the electron beam can drastically modify their evolution[9–13].

A comprehensive picture can only emerge from the combination of several methods[14–16], ideally representing the three main families of physical experimental techniques (imaging, scattering and spectroscopy). In this work we used a coupled approach, following the reshaping kinetics of gold NTPs in parallel via synchrotron-based SAXS and AS, in solution between 40 and 60°C. Complemented by ex situ transmission electron microscopy (TEM) analysis, these two in situ techniques are in very good agreement on the temperature dependence of the process. We also performed in situ heating high-resolution TEM (HRTEM) of dry particles, providing a visual illustration of the transformation processes at atomic resolution. Our combined results demonstrate that the reshaping trajectories are similar in both liquid and dry states, with the process being significantly faster in the former.

2 Results and discussion

HRTEM imaging revealed the detailed geometry of the NTPs and their monocrystalline structure: a few objects exhibit sharp tips (Figures 1A, 1B in the text and S9 in the Supporting Information), delimited by $\{100\}$, $\{110\}$ and $\{111\}$ facets, in agreement with the results of Chang *et al.*[3], but most of them have "blunt" arms, terminated by $\{110\}$ facets (Figure 1C and D). The most probable explanation is that the samples we used for HRTEM had already evolved with respect to the as-synthesized condition (see Figures S15 and S16). HRTEM observations along different zone axes (detailed in Figures S9-S11) confirm the established overall geometry of the NTPs, whose arms grow along $\langle 110 \rangle$ directions and form two pairs with perpendicular orientations, contained in two planes perpendicular to each other[3].

Immediately after synthesis, the NTP solutions are greenish blue and their AS spectrum exhibits a strong peak around 750 nm and a smaller one close to 520 nm: we denote them as "longitudinal" and "transverse", respectively, by analogy with the case of nanorods[17,18]. Unlike nanorods, however, the NTPs are metastable and –at room temperature– the onset of the reshaping process is already noticeable 30 min after synthesis (Figure 2A). With time, the longitudinal peak decreases in amplitude while blue shifting and the transverse one is reinforced. In the final state, only the second peak remains. This evolution is accompanied by a change in color (Figure 2B) reflecting the reshaping of the NTPs into isometric objects, as shown in the inset. TEM images taken at various times illustrate this process (Figure 2C): arm shortening leads to a roughly isometric final shape. While some sharp tips can be seen in the beginning, the arms are rounded or flattened in subsequent images. In the dry state, the particles evolve very similarly, but on much longer time scales: months, instead of days (see Figure S2).

These preliminary observations show that the arms become blunter and shorter with time. A more detailed

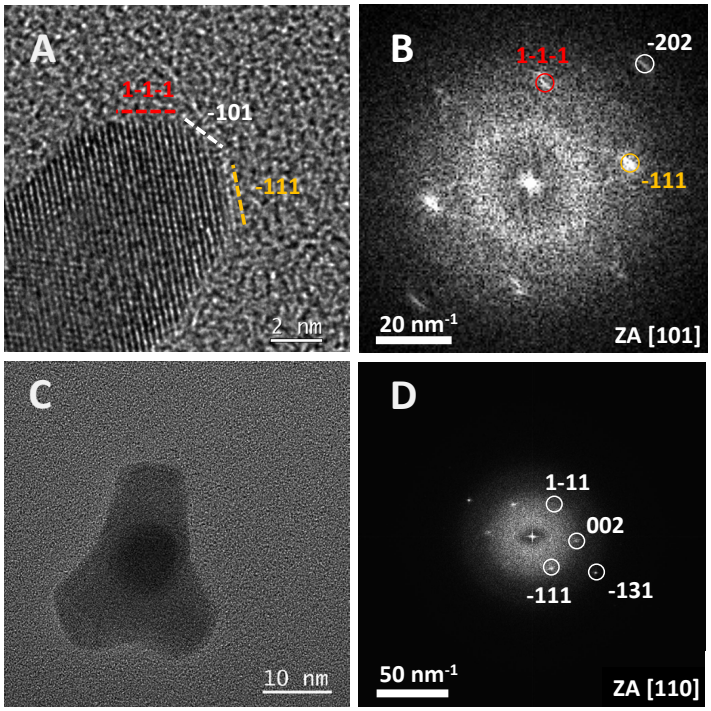

Figure 1 NTP structure. HRTEM image A) and corresponding Fourier transform B) of an NTP tip oriented along the [101] zone axis (ZA) and showing {111} and {110} facets. C) HRTEM image of an NTP observed along the [110] ZA and D) corresponding Fourier transform indexed with the FCC structure of gold.

analysis requires following the process in situ, but the room-temperature kinetics is very slow. To bring the reshaping time down to manageable values, we followed the process in situ at three different temperatures, between 40 and 60°C. Immediately after synthesis, the NTP solution was injected into the flow-through cell and transferred into a quartz cuvette, for SAXS/WAXS and AS measurements respectively. Both environments were pre-heated at the desired temperature and the time origin $t = 0$ was defined as the moment of injection into the X-ray setup or placement into the spectrophotometer. To minimize any discrepancies in evolution, these events were synchronized to within a few seconds.

The evolution of the extinction at $T = 50°$C is shown in Figure 3A: the spectra are color-coded according to the time scale on the right. All the spectra were combined into a two-dimensional matrix $\mathrm{A}_{\mathrm{exp}}(\lambda, t)$, indexed by wavelength and time. SVD analysis[19] of this data yielded the singular values W_{ii}, shown in Fig. 3B in order of decreasing amplitude. Since the first three values were clearly above the rest, we used only $K = 3$ basis spectra $\mathbf{S}_j(\lambda)$, with $j = \{1,..,K\}$ to create the model matrix $\mathrm{A}_{\mathrm{SVD}}(\lambda, t)$:

$$\mathrm{A}_{\mathrm{SVD}}(\lambda_m, t_n) = \sum_{i=1}^{K} \mathbf{C}_i(t_n)\mathbf{S}_i(\lambda_m) \tag{1}$$

We further imposed that the first and second basis spectra correspond to the starting and final model spectra: $\mathbf{S}_1(\lambda) = \mathrm{A}_{\mathrm{SVD}}(\lambda, t = 0)$, $\mathbf{S}_2(\lambda) = \mathrm{A}_{\mathrm{SVD}}(\lambda, t = t_{\mathrm{final}})$. They are shown in Fig. 3C as black and blue solid lines, respectively, and agree quite well with the corresponding experimental values (open dots of the same colors), validating the fidelity of the reconstruction. These spectra are therefore good descriptions of the AS signature of the initial and final states of the objects. Their amplitudes $\mathbf{C}_1(t)$ and $\mathbf{C}_2(t)$ (Fig. 3D) monotonically decrease and increase with time, respectively.

The third basis spectrum $\mathbf{S}_3(\lambda)$ (solid green line) was constrained to positivity and to having the same value at $\lambda = 400$ nm as the other two, reflecting the conservation of the amount of metallic gold in the solution[20]. It has a peak at an intermediate value with respect to them and its time variation is non-monotonic, with a steep increase followed by a slow decrease. We therefore assigned this spectrum to an intermediate species.

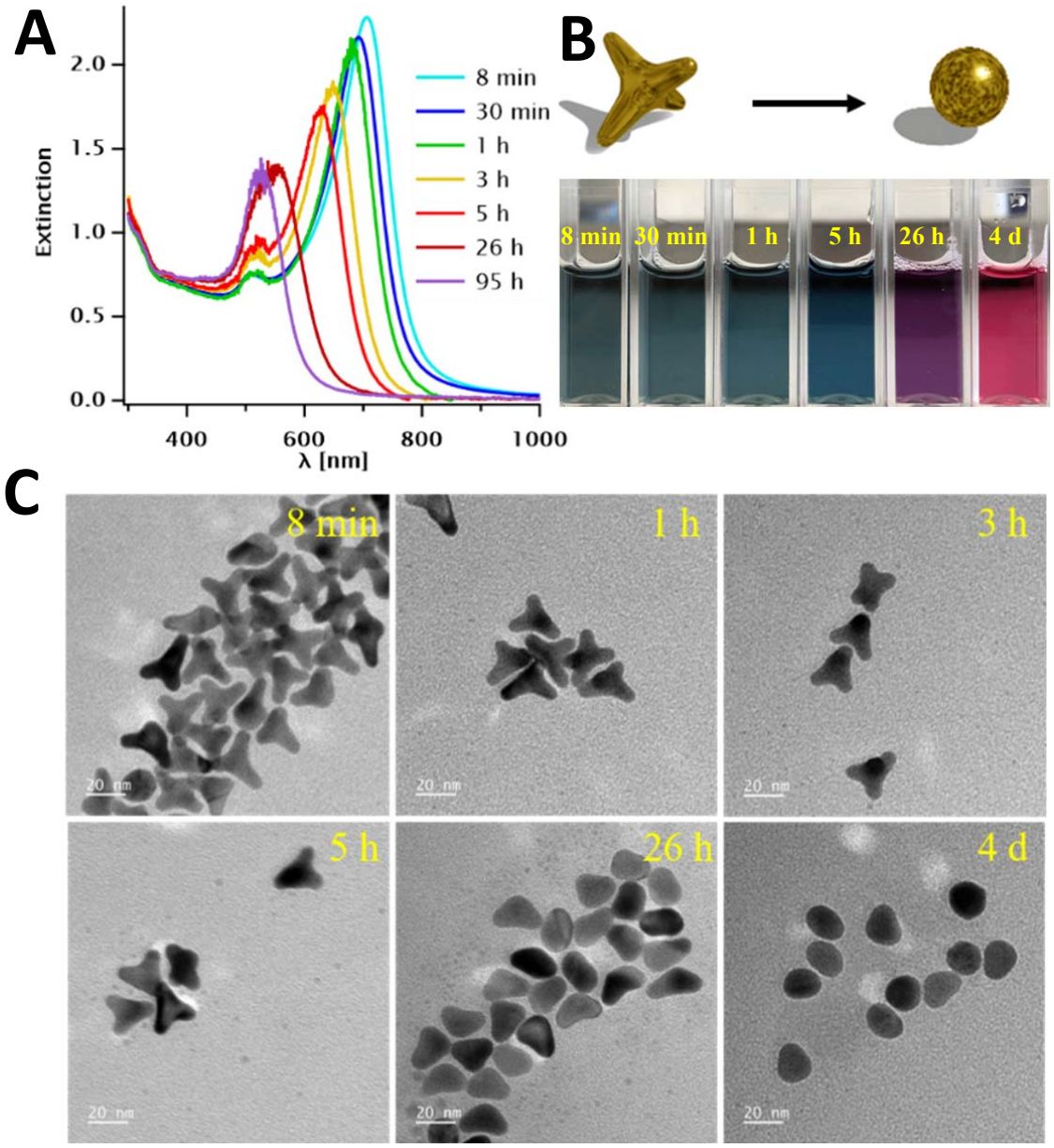

Figure 2 Structure and time evolution of the NTPs in solution. A) Time-resolved AS spectra and B) photographs of NTP suspensions during reshaping at $T = 20°$C. C) TEM images corresponding to some of the AS times. The scale bars represent 20 nm.

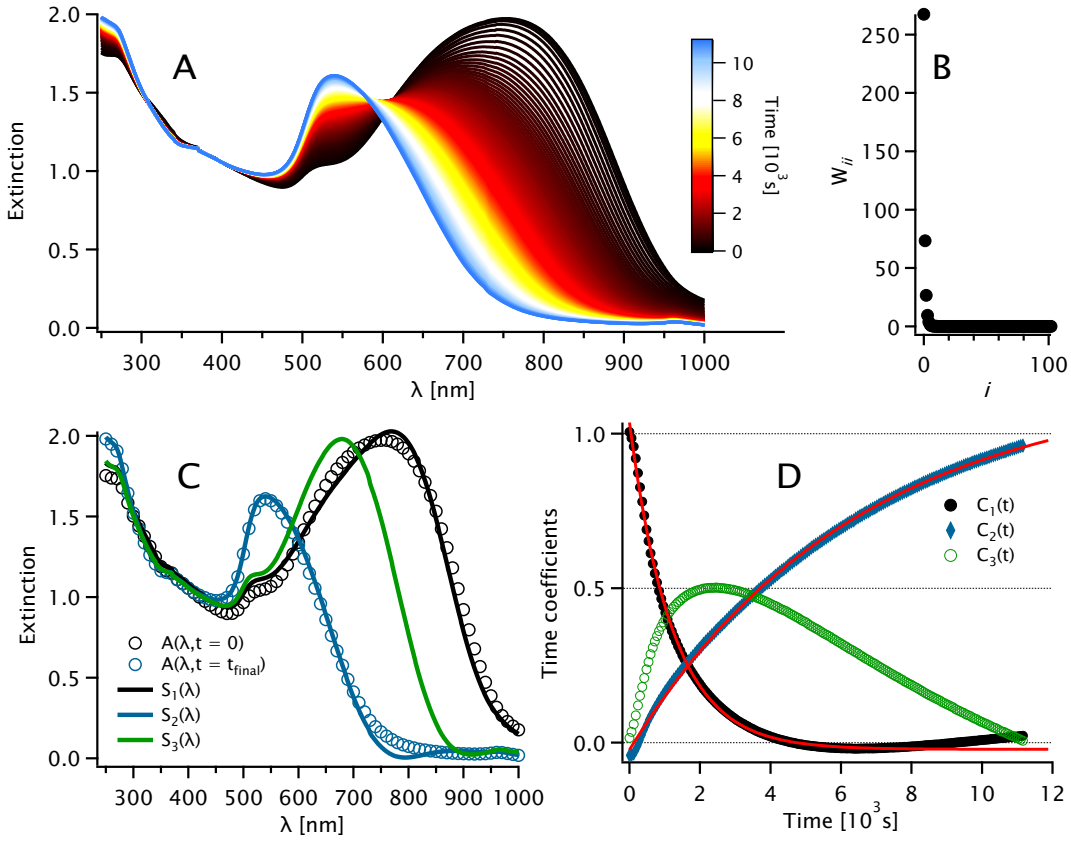

Figure 3 A) Time evolution of the AS spectrum $A(\lambda,t)$ at $T = 50°$C. B) Singular values W_{ii} as a function of the index i. C) SVD-extracted spectra of the three species $\mathbf{S}_k(\lambda)$, with $k = 1,2,3$ (black, blue and green line, respectively). The first and final experimental spectra are also shown for comparison (black and blue open dots, respectively). D) Time coefficients $\mathbf{C}_k(t)$ of the identified species (same color code as for the $\mathbf{S}_k(\lambda)$.) Exponential fits to the first two coefficients are shown as solid red lines (see the text for details).

Thus, the three time coefficients $\mathbf{C}_k(t)$ in Fig. 3D capture the full kinetics of the evolution from the starting (S) to the final (F) species, going through the intermediate (I) state:

$$\mathrm{S} \xrightarrow{\tau_1} \mathrm{I} \xrightarrow{\tau_2} \mathrm{F} \tag{2}$$

with characteristic times τ_i that can be estimated from exponential fits $\exp(-t/\tau_1)$ and $1-\exp(-t/\tau_2)$ to the coefficients $\mathbf{C}_i(t)$ (shown as red lines in Fig. 3D. These times are shown in Figure 4E for all three temperatures.

For a pointy and anisometric particle, both loss of sharpness and reduction in anisotropy translate into a blue shift of the absorbance spectrum, consistent with the evolution (2). Based on the TEM observations, the arm length and shape are relevant parameters, but it is difficult to obtain quantitative morphological information directly from the AS data. Scattering techniques are therefore needed to complete the picture.

The evolution of the SAXS intensity $I(q)$ at $T = 50°\mathrm{C}$ is shown in Figure 4A: the curves are color-coded according to the time scale (the same as in Figure 3). We fitted the data with the bead model shown in Fig. 4D (see also Figure S3) from which we extracted the arm length L and the core radius R_C as a function of time for the three temperatures studied. These parameters are shown in Figure 4 B and C, respectively. Other fit parameters are: the number density of particles n, the background bkg and the overall relative dispersity p. The number density starts at $n = 10^{-9}\,\mathrm{nm}^{-3}$ and decreases by the end of the kinetics by about 10% at 40 and 50°C and by about 25% at 60°C. At the same time, bkg increases linearly throughout the kinetics. These two effects could be correlated, and due to the dissolution of a small number of particles. Throughout the analysis p is set at 0.55, a value that optimizes the goodness of fit for all temperatures. An upturn is observed at very small q, probably due to slight particle aggregation, and becomes less pronounced with time as the dispersion state improves after temperature increase. To limit its effect we do not include in the fit the first 10 points (below the first dashed line in Figure 4A).

The most relevant parameter for the reshaping process is the arm length L, and thus we fitted its time evolution by an exponential decay : $L(t) = L_i \exp(-t/\tau) + L_f$. This dependence is similar to that of the AS data (see above), so we display in Figure 4E the decay times τ_1, τ_2 and τ obtained from both these methods, in an Arrhenius plot ($\log\tau$ vs $1/T$). τ is close to τ_2, so we conclude that our data captures only the second (arm shortening) step, but not the first one (arm blunting).

The values obtained from the two techniques are quite similar and follow Arrhenius laws: $\tau(T) \sim \exp\left(\frac{E_A}{k_B T}\right)$, with an activation energy $E_A = (0.98 \pm 0.1)\ \mathrm{eV} = (39 \pm 4)\ k_B T$, where the uncertainty was estimated from the slope of the three curves and the thermal energy $k_B T$ is taken at the normal temperature $T = 20°\mathrm{C}$. The fast and slow AS times τ_1 and τ_2 are about a factor 6 apart (see the model curves in Fig. 4E.)

As a reference for the evolution of the NTPs in solution, we have also studied their reshaping at the atomic scale via HRTEM . Since the as-synthesized NTPs suspensions could not be purified from excess reactant without significant reshaping, we opted to cover the NTPs with a thin Ag layer[4] to slow down the kinetics. Once the particles were in place, we heated the sample and followed the evolution of the NTPs. One such process is shown in Figure 5, at $T = 150°\mathrm{C}$ and a dose rate of 3000 $\mathrm{e}^-/\mathrm{s}/\mathrm{Å}^2$.

These in situ observations recapitulate at a faster rate the transformation mechanism of NTPs in solution that could be inferred from ex situ TEM images. As seen in Figure 5, the $\{110\}$ facets at the apex of the arms grow while the curvature of the concave surfaces decreases, indicating the transfer of atoms from the arm tips to the concave surfaces in-between the arms, whose chemical potential is lower. Consequently, the tips of the NTPs flatten out, their arms shorten and their core enlarges until the nanoparticle becomes roughly isometric. The effect of the Ag layer on the kinetics is unclear. Previous in situ TEM studies on the reshaping of AuAg nanoparticles have suggested that interdiffusion, rather than detachment of the Ag layer, occurs[21,22]. Based on these findings, the most consistent hypothesis involves an initial step of alloy formation, followed by surface diffusion.

We extracted the typical evolution time $\tau = (190 \pm 20)$ s by fitting the arm length vs. time with an exponential decay function: $L(t) = (L_i - L_f)\exp(-t/\tau) + L_f$, where L_i and L_f are the initial and final values, respectively.

At the same temperature $T = 150°\mathrm{C}$, reducing the dose rate by about a factor of three (to 1150 $\mathrm{e}^-/\mathrm{s}/\mathrm{Å}^2$) dramatically slows the reshaping process, as shown in Figure S13. Clearly, the dose rate has a strong influence on

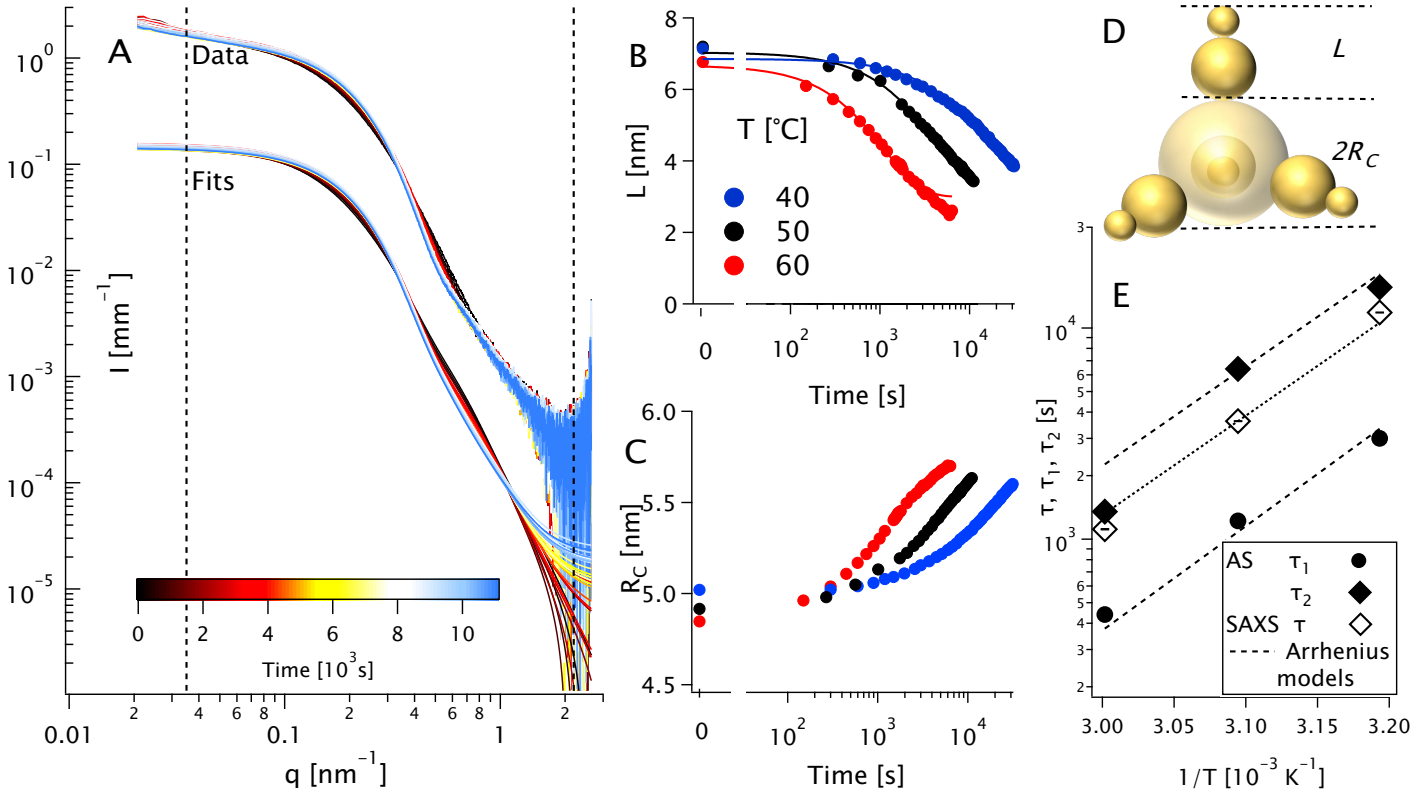

Figure 4 A) time evolution of the SAXS intensity $I(q)$ at $T = 50°$C (same sample kinetics as in Fig. 3, with the same color code). For clarity, the fits are shifted downwards by one decade with respect to the data. Only the q-range limited by the dashed lines is used for the fits. Time evolution of the arm length L B) and the core radius R_C C) obtained from the fit, for all temperatures. Error bars are smaller than the symbol size. For $L(t)$, double exponential fits are shown as full lines (see the text for more details). D) Bead model used for the fits in A). The two fit parameters L and R_C are illustrated. E) Arrhenius plot (time in log scale vs. reciprocal temperature) of the characteristic times τ_1 and τ_2 obtained via AS (solid symbols) and τ via SAXS (open symbols). Error bars are smaller than the symbol size. The dashed lines are Arrhenius models for τ_1 and τ_2 with the same activation energy $E_A = 0.98\,\text{eV} = 39\,k_BT$ and differing by a factor of 6. Dotted line is an Arrhenius model for τ with the same E_A.

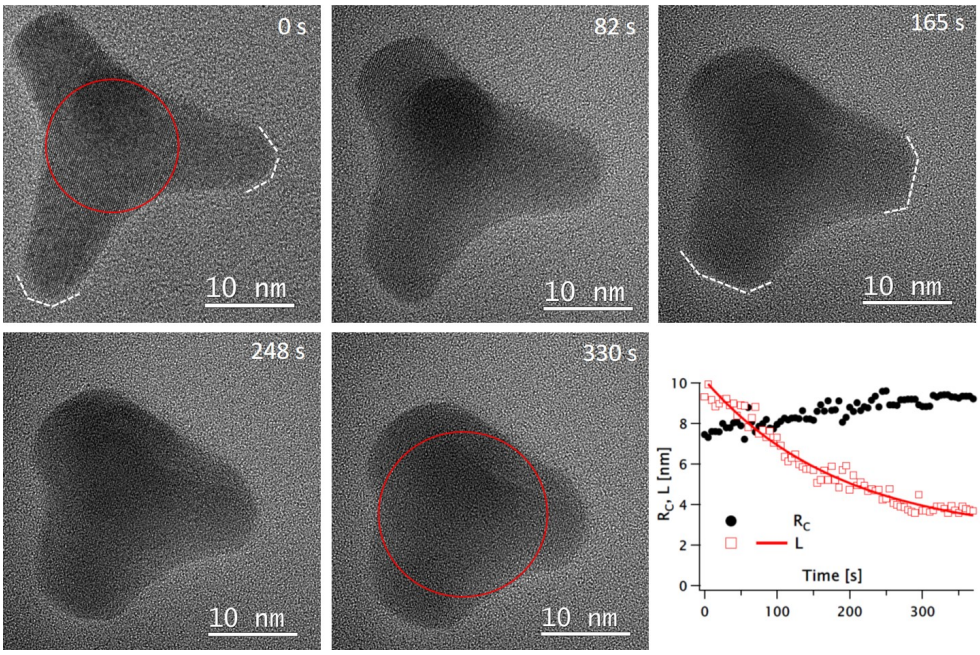

Figure 5 Reshaping of a dry NTP followed by in situ HRTEM at 150°C, under a dose rate of 3000 $e^{-}/s/Å^{2}$. The acquisition time is indicated in the top right corner of each image. The evolution of the tip faceting is highlighted with white dashed lines. The graph in the bottom-right section shows the measurement of the core radius and the arm length over time. The core of the NP is indicated with a red circle on the first and last images of the time series (see SI for details on the measurements of the arm length).

the kinetics. Conversely, we noted significant reshaping at $T = 300^{\circ}$C and an even lower dose rate (67 $e^{-}/s/Å^{2}$), see Figure S14. Although the conditions differed (in terms of temperature and dose rate) with respect to Figure 5, the two evolutions were remarkably alike. Even more significantly, the reshaping trajectories are similar in the liquid and the dry state, but on much slower time scales: the presence of the reaction medium is clearly essential for effective reshaping.

3 Conclusions

In conclusion, we monitored in situ the shape evolution of gold NTPs with a well-defined morphology at different temperatures using optical extinction spectroscopy and synchrotron-based X-ray scattering in parallel, on aliquots from the same reaction solution. We analyzed the data by singular value decomposition for the former technique and by full-curve fitting for the latter. These results, complemented by ex situ TEM measurements, can be explained by a two-step process: quick flattening of the tips into $\{110\}$ facets, followed by slow shortening of the arms. The characteristic times for the two stages differ by a factor of six but have the same activation energy, 0.94 eV, similar to that of surface diffusion[23,24].

The most likely mechanism for dry-state kinetics is surface migration of the gold atoms, as observed for dry-state gold nanostars[25] and octopods[26]. It is noteworthy that some objects investigated in these works seem to follow the same two-step process as the NTPs: fast tip blunting and slow retraction (see Fig. 2 of Ref. 25). We draw these conclusions independently: they are not stated by that paper's authors.

The much faster reshaping of NTPs in solution (in contrast to the dry state at the same temperature) is presumably CTAB-aided, as for nanostars[6]. We cannot conclusively infer that this is a dissolution-redeposition process, as stated by these authors, or surface diffusion facilitated by the liquid medium, as hinted at by the similarity in evolution and in activation energy with the dry-state process.

Besides a fundamental advance in understanding nanoparticle evolution, elucidating this mechanism also yields an effective way of predicting the optical properties of acicular nano-objects, with multiple potential applications in nanotechnology.

The following information is available free of charge:

- Materials and Methods
- Particle evolution in the dry state
- Details on the SAXS analysis
- WAXS results
- Additional HRTEM images and analysis
- In situ heating TEM: model and additional data
- Reference samples for TEM
- Video of the kinetics analyzed in Figure 5

Acknowledgements J. L. acknowledges financial support by the China Scholarship Council (CSC), the National Natural Science Foundation of China (No. 52301288), the Postdoctoral Science Foundation of Shaanxi Province (No. 2023BSHEDZZ260) and the Shaanxi Fundamental Science Research Project for Mathematics and Physics (Grant No. 23JSQ017). We acknowledge the ESRF for provision of synchrotron radiation facilities (project SC-5093) and the PSCM for the UV-Vis measurements. We thank Pierre Lloria for welcoming us at PSCM and Claire Goldmann for experimental support. This work is supported by the Agence Nationale pour la Recherche (ANR) via project METATRAP (ANR-22-CE09-0011-01).

References

[1] A. Guerrero-Martínez, S. Barbosa, I. Pastoriza-Santos and L. M. Liz-Marzán, *Current Opinion in Colloid & Interface Science*, 2011, **16**, 118–127.

[2] E. Hao, R. C. Bailey, G. C. Schatz, J. T. Hupp and S. Li, *Nano Letters*, 2004, **4**, 327–330.

[3] Y.-X. Chang, N.-N. Zhang, Y.-C. Xing, Q. Zhang, A. Oh, H.-M. Gao, Y. Zhu, H. Baik, B. Kim, Y. Yang, W.-S. Chang, T. Sun, J. Zhang, Z.-Y. Lu, K. Lee, S. Link and K. Liu, *The Journal of Physical Chemistry Letters*, 2019, **10**, 4505–4510.

[4] J. Lyu, F. Rondepierre, C. Jonin, P.-F. Brevet, C. Hamon and D. Constantin, *The Journal of Physical Chemistry C*, 2022, **126**, 9831–9835.

[5] P. Senthil Kumar, I. Pastoriza-Santos, B. Rodríguez-González, F. Javier García de Abajo and L. M. Liz-Marzán, *Nanotechnology*, 2008, **19**, 015606.

[6] L. Rodríguez-Lorenzo, J. M. Romo-Herrera, J. Pérez-Juste, R. A. Alvarez-Puebla and L. M. Liz-Marzán, *Journal of Materials Chemistry*, 2011, **21**, 11544.

[7] A. Kedia and P. S. Kumar, *Journal of Materials Chemistry C*, 2013, **1**, 4540.

[8] Y. Xianyu, Y. Lin, Q. Chen, A. Belessiotis-Richards, M. M. Stevens and M. R. Thomas, *Angewandte Chemie International Edition*, 2021, **60**, 9891–9896.

[9] X. Tian, U. Anand, U. Mirsaidov and H. Zheng, *Small*, 2018, **14**, 1803231.

[10] K. Aliyah, J. Lyu, C. Goldmann, T. Bizien, C. Hamon, D. Alloyeau and D. Constantin, *The Journal of Physical Chemistry Letters*, 2020, **11**, 2830–2837.

[11] A. Khelfa, J. Meng, C. Byun, G. Wang, J. Nelayah, C. Ricolleau, H. Amara, H. Guesmi and D. Alloyeau, *Nanoscale*, 2020, **12**, 22658–22667.

[12] A. Khelfa, J. Nelayah, H. Amara, G. Wang, C. Ricolleau and D. Alloyeau, *Advanced Materials*, 2021, **33**, 2102514.

[13] Z. Lyu, L. Yao, W. Chen, F. C. Kalutantirige and Q. Chen, *Chemical Reviews*, 2023, **123**, 4051–4145.

[14] S. Mourdikoudis, R. M. Pallares and N. T. K. Thanh, *Nanoscale*, 2018, **10**, 12871–12934.

[15] F. Schulz, I. Lokteva, W. J. Parak and F. Lehmkühler, *Particle & Particle Systems Characterization*, 2021, **38**, 2100087.

[16] P. T. Prins, J. C. Van Der Bok, T. P. Van Swieten, S. O. M. Hinterding, A. J. Smith, A. V. Petukhov, A. Meijerink and F. T. Rabouw, *Angewandte Chemie International Edition*, 2023, **62**, e202305086.

[17] L. Vigderman, B. P. Khanal and E. R. Zubarev, *Advanced Materials*, 2012, **24**, 4811–4841.

[18] H. Chen, L. Shao, Q. Li and J. Wang, *Chemical Society Reviews*, 2013, **42**, 2679.

[19] J. Lyu, D. Alloyeau, C. Hamon and D. Constantin, *Journal of Materials Chemistry C*, 2021, **9**, 1730–1739.

[20] T. Hendel, M. Wuithschick, F. Kettemann, A. Birnbaum, K. Rademann and J. Polte, *Analytical Chemistry*, 2014, **86**, 11115–11124.

[21] A. Skorikov, W. Albrecht, E. Bladt, X. Xie, J. E. S. Van Der Hoeven, A. Van Blaaderen, S. Van Aert and S. Bals, *ACS Nano*, 2019, **13**, 13421–13429.

[22] M. Mychinko, A. Skorikov, W. Albrecht, A. Sánchez-Iglesias, X. Zhuo, V. Kumar, L. M. Liz-Marzán and S. Bals, *Small*, 2021, **17**, 2102348.

[23] R. Hummel and H. Geier, *Thin Solid Films*, 1975, **25**, 335–342.

[24] T.-S. Lin and Y.-W. Chung, *Surface Science*, 1989, **207**, 539–546.

[25] H. Vanrompay, E. Bladt, W. Albrecht, A. Béché, M. Zakhozheva, A. Sánchez-Iglesias, L. M. Liz-Marzán and S. Bals, *Nanoscale*, 2018, **10**, 22792–22801.

[26] W. Albrecht, E. Bladt, H. Vanrompay, J. D. Smith, S. E. Skrabalak and S. Bals, *ACS Nano*, 2019, **13**, 6522–6530.